Analysis and Implementation of Transformerless *LCL* Resonant Power Supply for Ozone Generation

Muhammad Amjad, Zainal Salam, Mochammad Facta, and Saad Mekhilef, *Member, IEEE*

***Abstract*—This paper describes the analysis and design of an *LCL* resonant power supply for ozone generation. The main advantage of the proposed topology is the absence of high-voltage transformer; the high voltage gain is achievable by means of double-resonance phenomena. Furthermore, the bandwidth is wider than the ordinary *LC* and its phase difference is constant over specific frequency range; as a result, an open-loop operation can be implemented. The complete analysis and design procedure of the power supply is presented. The design procedure is verified by implementing the power supply to drive a dielectric barrier discharge prototype ozone chamber. The hardware results are found to be in close agreement with simulation and thus justify the validity of the design procedures. The proposed circuit is suitable for portable ozone power supply fed by low-voltage source such as battery or photovoltaic module.**

***Index Terms*—Dielectric barrier discharge (DBD), full-bridge inverter, high-voltage power supply, *LCL* resonant circuit, ozone generation.**

I. Introduction

THE use of ozone gas (O_3) has been increasing due to its excellent oxidizing properties. It is used in many diverse fields such as industries, agriculture, pharmaceutical, and water treatment. It exhibits strong antigermicidal properties, a characteristic that is useful for air and water purification [1]–[3]. In semiconductor industry, dissolved ozone in water is used for surface cleaning of device fabrication, as an alternative for sulphuric acid and ammonia-based mixtures [4]. It has been used in food processing industry as sanitizers. In hospitals, ozone is mainly used as disinfectant for surgical equipments, clothes, and linens. In agriculture, ozone is used for postharvest treatment to increase the shelf life and freshness of fruits, flowers, and vegetables [5].

Electrically, O_3 can be generated by breaking the oxygen molecules in a dielectric barrier discharge (DBD) chamber. The important property of the DBD is the creation of cold nonequilibrium plasma at atmospheric pressure condition. In a DBD chamber, a high ac voltage is applied between two electrodes, one of which is covered with dielectric. Oxygen is forced to flow in a space between the electrodes, called discharge gap. If the electric field is sufficiently high, it breaks the oxygen molecules into its atoms, the latter then combines with other oxygen molecules to form O_3. Traditionally, a low-frequency (50 Hz) ac source, coupled with a high turns-ratio transformer, is used as the power supply for the ozone generator [6], [7]. This approach requires high voltage across the chamber, since it must operate close to the discharge potential. Typically, a voltage in excess of 20 kV is necessary to create the breakdown for a 1-mm discharge gap [8], [9]. The high voltage limits the ozone production in several ways. First, it restricts the use of different dielectric materials due to the inability of these materials to withstand high-voltage stress. Second, the high voltage limits the discharge gap size, which in turn limits the amount of ozone gas that can be produced in the ozone chamber. Third, a low-frequency system is also associated with lower power conversion efficiency and larger power converter size.

To increase the ozone quantity, the chamber is fed by high-frequency power supplies. The high-frequency operation increases the power density applied to the electrode surface. This increases the ozone production for a given surface area, while decreasing the necessary peak voltage. At lower voltage, it is possible to experiment various types of dielectric materials with much lower voltage stress level. It is also more acceptable for domestic applications as it does not need special handling that is normally required for high-voltage equipment. In addition, the power supply using high-frequency technique has smaller footprint and higher efficiency.

Typically, high-frequency resonant inverters of various topologies are employed for ozone power supply. A step-up transformer is required because the gain ratio of the resonant circuit is insufficiently high to achieve the chamber breakdown voltage. In [10]–[14], a voltage-fed full-bridge resonant inverter with high-frequency inductor is proposed. The inductor is placed at the secondary [13], [14] or primary [11] side of the transformer to stabilize the discharge in the ozone chamber. In [15], a current-fed full-bridge inverter which employs a parallel inductor between the secondary and the ozone chamber is implemented. For the push–pull inverters proposed in [9] and [16]–[19], two inductors are used as chokes for the power supplies. In all the aforementioned topologies, the additional inductor, with value typically in millihenry, increases the cost and complexity of the circuit. Correspondingly, the equivalent series resistance of the inductor reduces the efficiency of the

Manuscript received January 30, 2012; revised April 6, 2012; accepted May 20, 2012. Date of current version September 27, 2012. This work was supported by Universiti Teknologi Malaysia through Vot. No. 79411. Recommended for publication by Associate Editor H. S. H. Chung.

M. Amjad is with the Universiti Teknologi Malaysia, Johor Bahru 81310, Malaysia, and also with the University College of Engineering and Technology, The Islamia University of Bahawalpur, Bahawalpur 63100, Pakistan (e-mail: muhammad.amjad@iub.edu.pk).

Z. Salam (corresponding author) and M. Facta are with the Universiti Teknologi Malaysia, Johor Bahru 81310, Malaysia (e-mail: zainals@fke.utm.my; mochfacta@gmail.com).

S. Mekhilef is with the Department of Electrical Engineering, University of Malaya, Kuala Lumpur 50603, Malaysia (e-mail: saad@um.edu.my).

Color versions of one or more of the figures in this paper are available online at http://ieeexplore.ieee.org.

Digital Object Identifier 10.1109/TPEL.2012.2202130

power supply. In [20]–[22], ozone power supply using class-E resonant inverter is presented. However, it is observed that the voltage waveform across the chamber is nonsinusoidal. The reported efficiency of the power supply is approximately 50%, which limits the use of this topology in low-power applications.

Since these power supplies utilize high turn ratio transformer, the associated leakage inductance results in high voltage spike across the switch during commutation. This results in low-switch utilization factor. Furthermore, the use of protection circuit is necessary to avoid destruction of the switch, thus increasing the cost and complexity [19]. Another disadvantage of transformers is the electromagnetic interference, particularly at high frequency. Furthermore, the core saturation limits the frequency range of operation. Although piezoelectric transformer (PT) is introduced to alleviate some of these problems, its bandwidth at resonance is extremely narrow; as a result, a closed-loop control is mandatory [23], [24]. Furthermore, a high step-up ratio PT with reasonably high power rating is not readily available in the market.

Most DBD chambers are constructed using fragile but thick (1–4 mm) dielectric materials. Commonly used materials are glass and alumina ceramic. Due to the thickness, they exhibit high dielectric breakdown voltages [25], [26]. Theoretically, the initiation voltage, i.e., the voltage that initiates the ozone generation, is close to its breakdown voltage; for a typical chamber using glass as dielectric with discharge gap of 1 mm, the initiation voltage is about 10–20 kV [4], [27]. Recently, the use of mica as dielectric in ozone chamber has been reported [28], [29]. The main advantage of mica is the low initiation voltage; for the same discharge gap size, the initiation voltage is approximately one order of magnitude less than glass. This is primarily due to the fact that mica is flexible, agile, and not easily breakable, hence can be readily constructed with thickness of less than 0.5 mm. The lower initiation voltage opens the possibility of developing ozone power supply without a transformer, i.e., transformerless ozone generator. This opportunity is explored in this study.

With the absence of a transformer, the voltage gain of the power supply is achieved only by the means of the *LC* resonant tank circuit [30], [31]. However, for an ordinary *LC* circuit, a sufficiently high voltage gain cannot be achieved unless the power supply is fed by the single- or three-phase utility supply [32]. This restricts the availability of the ozone generator to premises with utility power outlets. In [33], a high gain is achieved by employing resonant transformer made up by discrete inductors and capacitors, to achieve a transformer-like voltage gain. This solution requires more components, thus increasing the reactive power requirement. Furthermore, if an *LC* circuit feeds an inductive or capacitive load, the typical power factor is very low, i.e., less than 0.1 [34]. Considering these factors, a transformerless ozone generator based on *LCL* resonant tank is proposed. The main advantage of this topology is that the gain is much higher and its resonant bandwidth is wider than the ordinary *LC*. Furthermore, if correctly designed, the output current of the power supply can be almost independent of the load. Although the power supplies based on *LCL* circuit for inductive power transfer (inductive charging) are implemented in [34]–[37], no literature has reported its application for capacitive load such as the DBD ozone chamber. *LCL* circuit for resistive load is widely described elsewhere [38], [39].

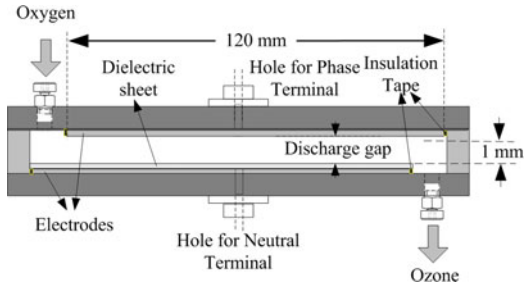

Fig. 1. Ozone chamber configuration.

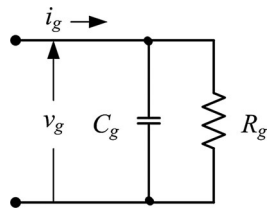

Fig. 2. Linear model of ozone chamber.

The objective of this paper is to describe the concept, design, and implementation of the *LCL*-based high-voltage power supply for ozone generation. The *LCL* tank achieves double resonance, which makes its gain much higher than the ordinary *LC* circuit. Thus, it can be suitably used for ozone power supply fed by low-voltage source such as battery or solar photovoltaic module. The phase difference between voltage and current is constant over a specific range of frequency; as a result, a closed-loop operation is not required. With the elimination of the transformer, the power supply size is reduced and its efficiency is increased.

The remaining of this paper is organized as follows. In Section II, the ozone chamber parameter determination is explained. In Section III, the analysis of *LCL* resonant circuit with chamber parameters is described. The design procedure is discussed in Section IV. Experimental setup is described in Section V. Simulation and experimental results are given in Section VI. Finally, the conclusion is made in Section VII.

II. Parameter Determination of Ozone Chamber

The configuration of the DBD ozone chamber used in this study is shown in Fig. 1 [40]. It consists of two plane electrodes: one is made of aluminium mesh and the other is from copper. The length and width of each electrode is 120 mm $\times$ 70 mm, respectively. The muscovite mica with 0.1-mm thickness is used as the dielectric in the chamber. The discharge gap between the electrodes is 1 mm. Since the ozone chamber is considered as capacitive a load [19], the high-frequency linear model of ozone chamber is represented by a parallel combination of resistor R_g and capacitor C_g, as shown in Fig. 2 [41]. The power dissipated in R_g represents the power supplied to the ozone chamber [42].

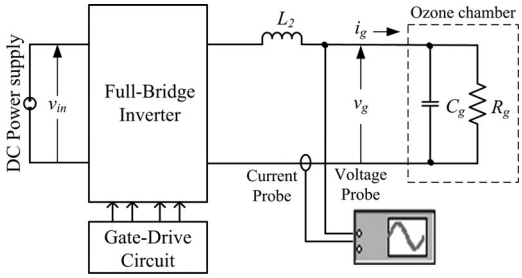

Fig. 3. Measurement setup for chamber parameter determination.

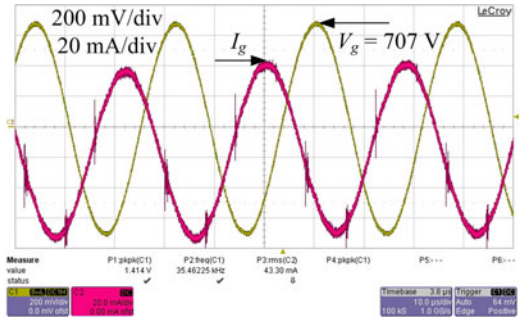

Fig. 4. Voltage and current waveforms of ozone chamber at frequency of 35.5 kHz. Note: measurements are carried out using the LeCroy 64Xi, 600 MHz, 10 GS/s digital oscilloscope equipped with a high-voltage probe and a high-frequency current probe.

It is necessary to know the parameters of the chamber equivalent circuit (in Fig. 2) at a specific frequency to facilitate the design of the high-voltage high-frequency power supply. The measurement setup to determine these parameters is shown in Fig. 3. The known value of an external inductor L_2 is placed between the inverter and the chamber to form a parallel-loaded resonant circuit. If the input signal frequency is equal to the resonant frequency, a high voltage gain is obtained. The transfer function of this circuit is given by

$$A_v = \left|\frac{V_g(j\omega)}{V_{\text{in}}(j\omega)}\right| = \frac{1}{\sqrt{(1-(\omega/\omega_p)^2)^2 + (\omega/\omega_p Q_p)^2}} \quad (1)$$

where ω_p is the undamped natural frequency and Q_p is the loaded quality factor, given by

$$\omega_p = \frac{1}{\sqrt{L_2 C_g}} \quad (2)$$

$$Q_p = \frac{R_g}{\omega_p L_2} = \omega_p C_g R_g. \quad (3)$$

The resonant frequency ω_r and the voltage gain A_{vm} at this frequency can be computed as

$$\omega_r = \omega_p \sqrt{1 - \frac{1}{2Q_p^2}} \quad (4)$$

$$A_{vm} = \frac{Q_p}{\sqrt{1 - \frac{1}{4Q_p^2}}}. \quad (5)$$

For $Q_p \gg 1$ (which is typical), (4) and (5) can be reduced to

$$\omega_r \cong \omega_p \quad (6)$$

$$A_{vm} \cong Q_p. \quad (7)$$

The C_g and R_g of the circuit can be calculated by combining (2) and (6), (3) and (7), respectively, resulting in the following equations:

$$C_g = \frac{1}{\omega_r^2 L_2} \quad (8)$$

$$R_g = A_{vm}\omega_r L_2. \quad (9)$$

For the ozone chamber described previously, the gate drive circuit provides a stable ac sweep gating signal to the inverter. The switching frequency of the inverter is varied slowly by the gate drive circuit until resonance is achieved. With $L_2 =$ 128.3 mH and $V_{\text{in}} = 45$ V, the experimental resonant frequency is 35.5 kHz. The voltage and current waveforms at resonance are illustrated in Fig. 4. Note that for every L_2C_g parallel-loaded combination, there exists a unique resonant frequency. Furthermore, from (8), the value of C_g is independent of chamber voltage. The computed value of C_g is 157.1 pF. The experimental results show that A_{vm} is constant at different input voltages, which is consistent with (9). Accordingly, R_g is also independent of chamber voltage and computed to be 391.9 kΩ.

It is known that R_g and C_g are frequency dependent [11]. However, as recently proven in [40], the variation of C_g (using the same chamber) is extremely small, i.e., in tens of picofarad. For that reason, it can be deduced that the variation of C_g on the voltage gain and resonant frequency is not significant. For the chamber resistance, its variation has no effect on resonant frequency. However, it does affect the chamber voltage; if the chamber resistance increases, the output voltage also increases and vice versa.

III. Analysis of *LCL* Resonant Circuit

A. Frequency-Domain Analysis

The proposed series–parallel ($L_1C_1L_2$) resonant circuit connected to ozone chamber is shown in Fig. 5. Effectively, it behaves like two parallel-loaded circuits, i.e., L_1C_1 and L_2C_g are connected in series (cascaded) to achieve double-resonance phenomena. The idea is to achieve sufficiently high gain so that the transformer can be omitted. Although the input to the resonant circuit is a quasi-square (fed from the inverter), the voltages v_1 and v_g are sinusoidal. The input impedance of the circuit is given by

$$Z_{\text{in}} = \frac{a_1 s^4 + a_2 s^3 + a_3 s^2 + a_4 s + a_5}{b_1 s^3 + b_2 s^2 + b_3 s + 1} \quad (10)$$

where

$$a_1 = L_1L_2C_1C_gR_g, \quad a_2 = L_1L_2C_1$$
$$a_3 = L_1C_gR_g + L_1C_1R_g + L_2C_gR_g$$
$$a_4 = L_1 + L_2, \quad a_5 = R_g, \quad b_1 = L_2C_1C_gR_g$$
$$b_2 = L_2C_1, \quad b_3 = C_gR_g + C_1R_g.$$

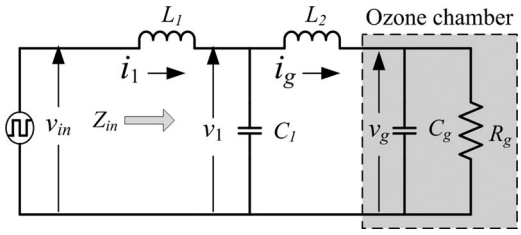

Fig. 5. $L_1C_1L_2$ resonant circuit and ozone chamber parameters.

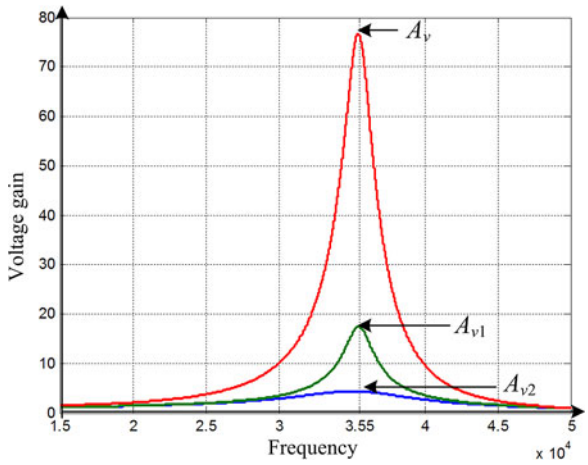

Fig. 6. Voltage gain of $L_1C_1L_2C_g$ circuit versus frequency.

The purpose of the L_1C_1 circuit is to provide significant voltage gain to the L_2C_g circuit. This is necessary as the gain of the latter is small. Furthermore, it provides the reactive current drawn by the L_2 and the chamber. The gains A_{v2} due to L_2C_g and A_{v1} due to L_1C_1 can be derived as

$$A_{V2} = \frac{v_g}{v_1} = \frac{R_g}{L_2C_gR_gs^2 + L_2s + R_g} \tag{11}$$

$$A_{V1} = \frac{v_1}{v_{\text{in}}} = \frac{a_6s^2 + a_7s + a_5}{b_4s^4 + b_5s^3 + b_6s^2 + b_7s + a_5} \tag{12}$$

where

$$a_6 = L_2C_gR_g, \quad a_7 = L_2$$
$$b_4 = L_1L_2C_1C_gR_g, \quad b_5 = L_1L_2C_1$$
$$b_6 = L_1C_1R_g + L_1C_gR_g + L_2C_gR_g, \quad b_7 = L_1 + L_2.$$

The overall voltage gain A_v of the chamber is given by

$$A_v = \frac{v_g}{v_{\text{in}}} = A_{v1} \times A_{v2}. \tag{13}$$

Note that L_2 is integrated with C_g to obtain the voltage gain A_{v2} at resonance. Additionally, the values of L_1 and C_1 are calculated so that the voltage gain A_{v1} is maximum at the same resonant frequency. The high voltage gain will be achieved due to double resonance, as depicted in Fig. 6.

Fig. 7(a) and (b) shows the phase variation of voltage and current waveforms with respect to the frequency for the proposed $L_1C_1L_2$ and the normal L_1C_1 resonant circuits, respectively. As can be seen, the phase difference for proposed circuit is constant

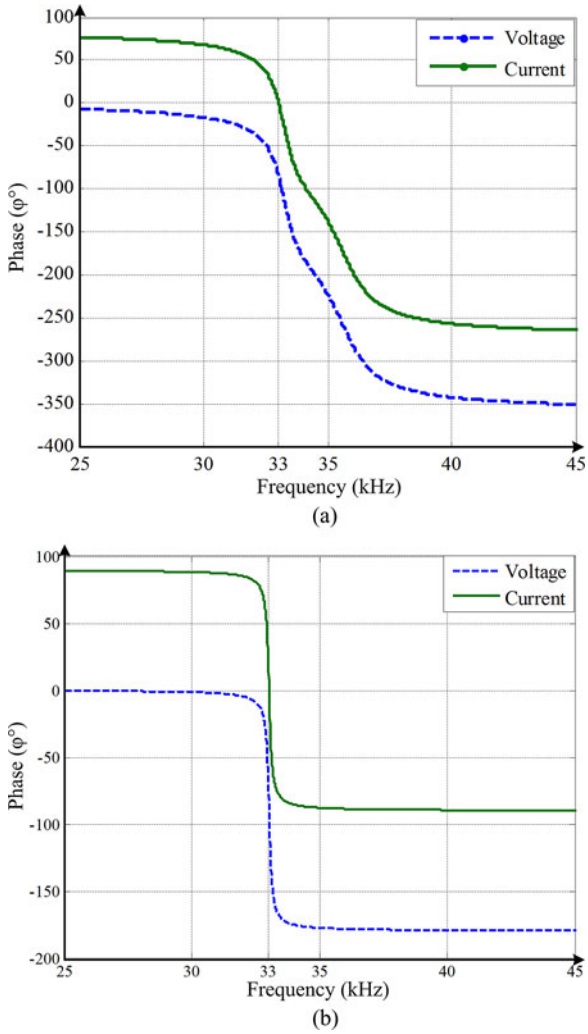

Fig. 7. Phase variation of chamber voltage and current waveforms of (a) proposed $L_1C_1L_2$ resonant circuit and (b) normal L_1C_1 resonant circuit.

over the range of frequency in which the gain is high, i.e., 33–35 kHz. The advantage of a constant phase difference is that the inverter switching frequency can be selected in this frequency range to achieve high voltage gain using only a loop control. In contrast, for the normal L_1C_1 circuit, the phase difference has a minimum value only at one frequency point, i.e., at 33 kHz. Furthermore, since the ozone chamber is a capacitive load with a low power factor, L_2 is connected in series with the chamber to compensate for the reactive power and to improve the power factor. As a result, it increases the power supplied to the chamber and consequently, the efficiency of the power supply is increased.

B. Time-Domain Analysis

The state-space equations of the $L_1C_1L_2$ circuit and equivalent chamber parameters (see Fig. 5) are developed to understand the relation between the input voltage, the current of the circuit, and the output chamber voltage. The state variables such as voltage across the capacitors and current of inductors are introduced, as shown in Fig. 4. The analysis is based on the assumption that

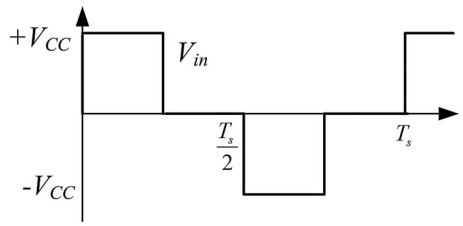

Fig. 8. Ideal output voltage of the inverter applied to the $L_1C_1L_2$ resonant circuit.

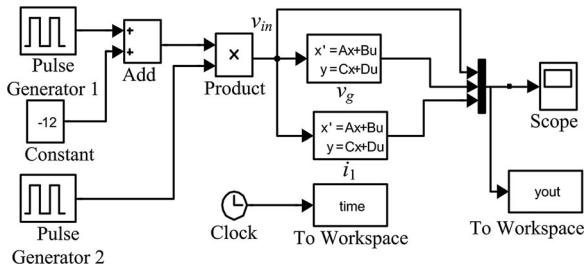

Fig. 9. State-space model using MATLAB/Simulink.

the components of the resonant circuit are ideal. Furthermore, to increase the efficiency of the power supply, the class DE inverter control with 25% duty factor is implemented [43]. The input voltage to the $L_1C_1L_2$ resonant circuit employing a 25% duty factor is shown in Fig. 8.

The four state equations that describe the time behavior of the circuit in Fig. 5 can be written as

$$\frac{dv_1}{dt} = \frac{1}{C_1}i_1 - \frac{1}{C_1}i_g \tag{14}$$

$$\frac{dv_g}{dt} = \frac{1}{C_g}i_g - \frac{1}{C_gR_g}v_g \tag{15}$$

$$\frac{di_1}{dt} = \frac{1}{L_1}v_{\text{in}} - \frac{1}{L_1}v_1 \tag{16}$$

$$\frac{di_g}{dt} = \frac{1}{L_2}v_1 - \frac{1}{L_2}v_g. \tag{17}$$

The state-space equation is derived as

$$\frac{d}{dt}\begin{bmatrix} v_1 \\ v_g \\ i_1 \\ i_g \end{bmatrix} = \begin{bmatrix} 0 & 0 & \frac{1}{C_1} & -\frac{1}{C_1} \\ 0 & -\frac{1}{C_gR_g} & 0 & \frac{1}{C_g} \\ -\frac{1}{L_1} & 0 & 0 & 0 \\ \frac{1}{L_2} & -\frac{1}{L_2} & 0 & 0 \end{bmatrix} \cdot \begin{bmatrix} v_1 \\ v_g \\ i_1 \\ i_g \end{bmatrix} + \begin{bmatrix} 0 \\ 0 \\ \frac{1}{L_1} \\ 0 \end{bmatrix} \cdot [v_{\text{in}}]. \tag{18}$$

Using (18) and utilizing the parameters from the measurements, the MATLAB/Simulink simulation model predicts the transient behavior of the circuit. The model is shown in Fig. 9. The input waveforms of voltage v_{in}, the input current i_1 of the circuit, and the output voltage v_g are plotted, as shown in Fig. 10. If the inverter is operated above the resonant frequency of the $L_1C_1L_2$ circuit, the MOSFETs switch softly prior to the zero crossing of the inverter output current i_1 and the zero voltage switching (ZVS) condition can be achieved. These waveforms also show the phase difference angle between the input voltage and the current.

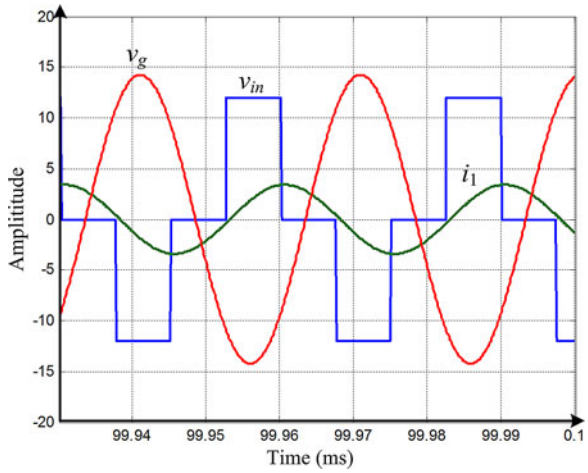

Fig. 10. Simulated input voltage v_{in}, input current i_1, and output voltage v_g.

IV. Design

To illustrate the application of the proposed $L_1C_1L_2$ circuit, the DBD chamber described in Section II is used. The values of L_1 and C_1 are calculated to obtain maximum voltage of 4 kVp-p across the chamber because the experimental test shows that this DBD chamber can withstand the maximum voltage of 4 kVp-p without experiencing the dielectric breakdown. If the $L_1C_1L_2$ circuit is fed by an inverter with maximum input voltage of 12 V, the required voltage gain is 166.7 (i.e., 2 kVp/12). The voltage gain due to L_2C_g (A_{v2}) is maximum at 35.5 kHz. However, if the values of L_1 and C_1 are calculated to provide the maximum gain A_{v1} at the same frequency, the resonant curve would be very narrow and the closed-loop operation would be mandatory. For an open-loop operation, L_1 and C_1 are calculated to provide the maximum voltage gain at 33 kHz. As the operating frequency of the inverter is selected to be higher than the resonance of the circuit, the overall voltage gain A_v should be higher than 166.7 at resonance. From the plot in Fig. 11, the value of A_{v2} at 33 kHz is 7. To calculate the values of L_1 and C_1, choose $A_{v1} = 50$, and $f = 33$ kHz. These values are substituted into (10) and (12). The input impedance of the circuit is zero at the resonance condition (12). By solving (10) and (12), the values of L_1 and C_1 are computed to be 820.1 μH and 27.5 nF, respectively. Based on these calculated values, the voltage gains A_{v2}, A_{v1}, and A_v are plotted in Fig. 11. As can be seen, the A_v at the frequency of 33 kHz is equal to the product of A_{v2} and A_{v1} and the voltage

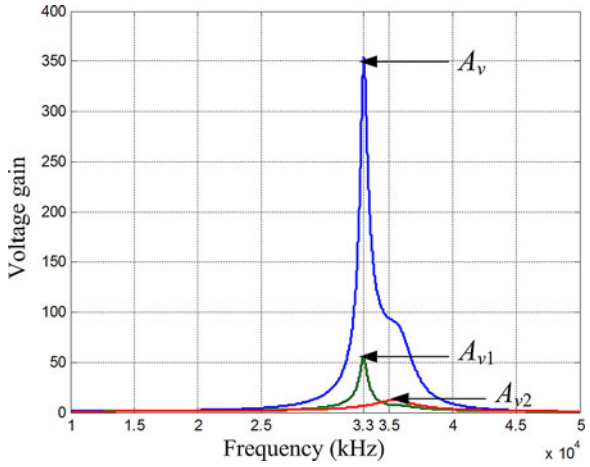

Fig. 11. Voltage gain $A_{v\,2}$, $A_{v\,1}$, and A_v of the $L_1C_1L_2$ circuit versus frequency.

gain at the frequency 33.4 kHz (i.e., the operating frequency) is 180.

With regard to component variations, if the combinational values of $L_1C_1L_2$ are varied within $\pm 10\%$ of the designed values, it will affect the resonant frequency. However, the maximum gain is almost constant because the gain is mainly dependent on chamber resistance R_g.

V. Experimental Setup

A. Full-Bridge Inverter and Gate Drive Circuit

The experimental setup of ozone generation system is shown in Fig. 12. For the bridge circuit, IRFP460 MOSFETs is used. The device is equipped with a freewheeling diode. The full-bridge MOSFETs M_1, M_3 and M_2, M_4 are switched in antiphase to produce quasi-square wave input excitation (V_{in}). The gate drive circuit that provides the switching signal for MOSFETs consists of LM3524D pulse width modulator (PWM), SN7407 buffer, and HCPL-3120 optocouplers. The circuit is shown in Fig. 13. The frequency of the gate drive signal is controlled by fixing a value for C at 0.1 μF (connected to pin C_t of the PWM IC) while adjusting the value of R from 0–200 kΩ (using pin R_t). These values provide stable ac sweep signals up to 100 kHz. Using the method, the use of phase-locked loop can be omitted.

B. Resonant Circuit

The calculated value of resonant capacitance C_1 is 27.5 nF. The maximum operating voltage of the resonant capacitance equal to V_1 is 4 kVp-p, at the resonant frequency. The high-voltage capacitors are not available easily. Therefore, the resonant capacitance is implemented by series connection of medium voltage and low equivalent series resistance capacitors. Eight polypropylene capacitors of 0.22 μF nominal capacitance, equivalent series resistance of 0.0616 Ω, and 300 V rated voltage are connected in series, resulting in equivalent capacitance of 27.5 nF. The series connection of capacitors can properly support the required operating voltage; as a result, the voltage of each capacitor becomes 250 Vp (i.e., 2 kVp / 8).

The desired values of resonant inductances are $L_1 = 820.1$ μH and $L_2 = 142.3$ mH. The voltage of the inductors is approximately equal to 4 kVp-p. This high voltage is not appropriate for enameled copper wire; as a result, additional interlayer insulation is used. The high-frequency inductors are designed in accordance with an area product approach. For implementation of L_1 and L_2, the ETD-44 and ETD-59, 3C90 ferrite cores are used, respectively. Finally, the desired values of resonant inductances are obtained by adjusting the air gap between the cores.

VI. Simulation and Experimental Results

To prove the viability of the proposed voltage multiplication method, the power supply using the designed values is implemented. To check the validity of obtained parameters, the circuit is simulated in MATLAB/Simulink. The resonant frequency of the circuit is 33 kHz. In order to achieve ZVS, the switching frequency of the inverter is set slightly above the resonant frequency of the circuit i.e., at 33.4 kHz. To control the output voltage (in order to avoid dielectric rapture), the following procedures are adopted during the experimental work. First, at low input voltage (say 3 V), the switching frequency is adjusted at 33.4 kHz by adjusting R in the gate drive circuit; this frequency is kept constant throughout the experiment. Then, the output voltage is increased by slowly increasing the input voltage of the inverter between 3 and 12 V. This is to ensure that the output voltage will not exceed the dielectric breakdown limit.

Fig. 14 illustrates the sinusoidal current and the voltage waveform of the ozone chamber at various input voltages. As can be seen, the current leads the voltage for all the operations because the chamber behaves as a capacitive load. With the increase in chamber voltage, the microdischarges in the current waveform of the chamber increases, resulting in an increase in the ozone generation. The simulated and experimental voltage and the current waveforms are in good agreement, which confirms that the obtained ozone chamber model parameters are valid.

Fig. 15 shows the chamber voltage as a function of inverter input voltage. As can be seen, the simulation results of the output voltage are linear throughout the input voltage range (3–12 V). Similar trend is observed when the inductor resistance is included in the simulation model. The difference is in the voltage drop due to the resistance that causes the drop in the output voltage. For the experimental results, the voltage across the chamber increases linearly up to the input voltage of 8 V (which corresponds to the output voltage of 3kVp-p). There is a slight difference in the simulation and experimental results beyond 3kVp-p due to the saturation that occurs inside the chamber. This phenomenon is consistent with the observations made by other researchers [9], [44]. The winding resistance of L_1 and L_2 are 1.4 Ω and 5.1 Ω, respectively. The maximum loss in L_1 is 800 mW, while in L_2 the loss is 25 mW.

Fig. 16 shows the plot for the efficiency of power supply against the chamber output power. The input power of the inverter is measured by Voltech PM6000 power analyzer. The phase difference between the voltage and the current waveforms (which are sinusoids) of the chamber is measured by an

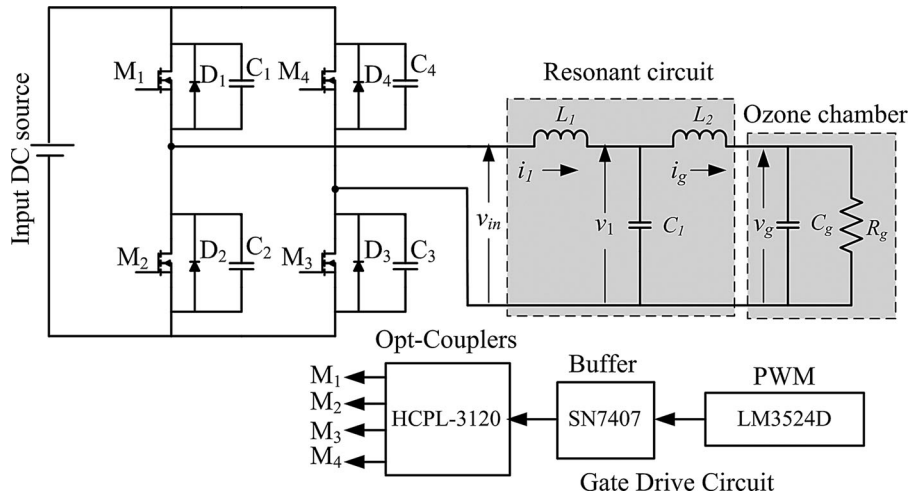

Fig. 12. Experimental setup.

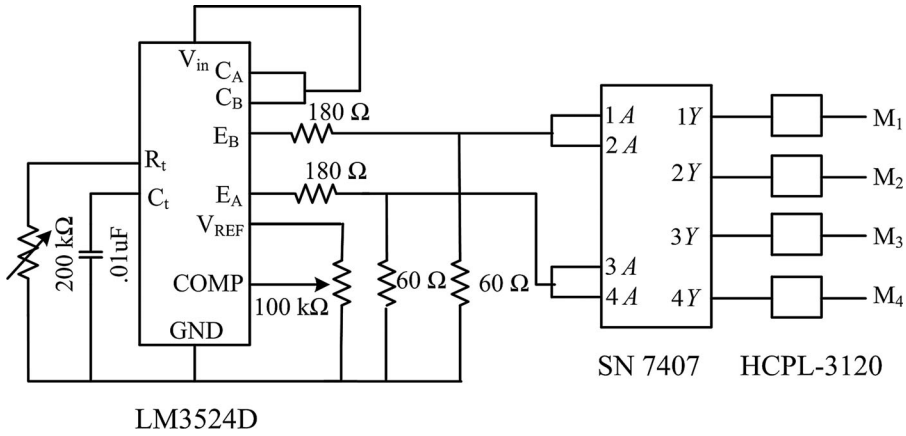

Fig. 13. Gate drive circuit.

oscilloscope. The output power of the chamber is calculated by multiplying the power factor and voltage–current [32]. The maximum inverter efficiency achieved is about 92% at the chamber power of 6.5 W. This efficiency is high when compared to other works (see, for example, [11], [20], and [45]).

Fig. 17 illustrates the ozone quantity as a function of input voltage. The ozone chamber is fed with 95% oxygen with flow rate of 1 L/min. The ozone quantity can be controlled by varying input dc voltage. The ozone concentration is measured using the InDevR 2B Technologies, UV 106 ozone monitor at scale of μg/m^3. The ozone quantity is calculated from the measured ozone concentration. The maximum ozone quantity obtained is 7.2 gO_3/h. This value is considered high compared to other ozone generators in the same category [20], [46].

Fig. 18 shows the ozone efficiency as a function of input voltage. The input power is measured to calculate the ozone efficiency. As can be seen, the maximum ozone efficiency of 62.87 gO_3/kWh is obtained at the input voltage of 10 V. As the input increases above 10 V, the power supplied to the ozone chamber increases. However, the power increases the temperature in the ozone chamber, thus decreasing the efficiency [9]. This ozone quantity is sufficient for many applications, for example, airborne ozone disinfection systems, storage and packing of fruits and vegetables, etc. [3], [5].

Fig. 19 compares the efficiency of the proposed $L_1C_1L_2$ circuit with three transformer-based power supplies for ozone generation system presented by previous researchers. It has to be noted that comparing the efficiencies of different topologies is quite difficult for two reasons: 1) the operating conditions of the power supplies, such as input voltage, power rating, and switching frequency are markedly different and 2) there exist variations in components values and types, as their thermal and electrical characteristics are not same. Despite these diversities, three transformer-based topologies that are closely related to this study are cited to gain some insight on the performance of the proposed power supply. From [20], the reported measured maximum efficiency of the class-E inverter is 50%, while the maximum efficiency of the power supply based on push–pull topology is 78% [16]. In another work [11], the authors have reported a maximum efficiency of 87% for full-bridge topology. Moreover, for high-voltage transformer, its secondary resistance is typically in order of hundreds of ohms [11]. For that reason, the losses are significantly higher. On the other hand, the winding resistance of inductors used in the transformerless power

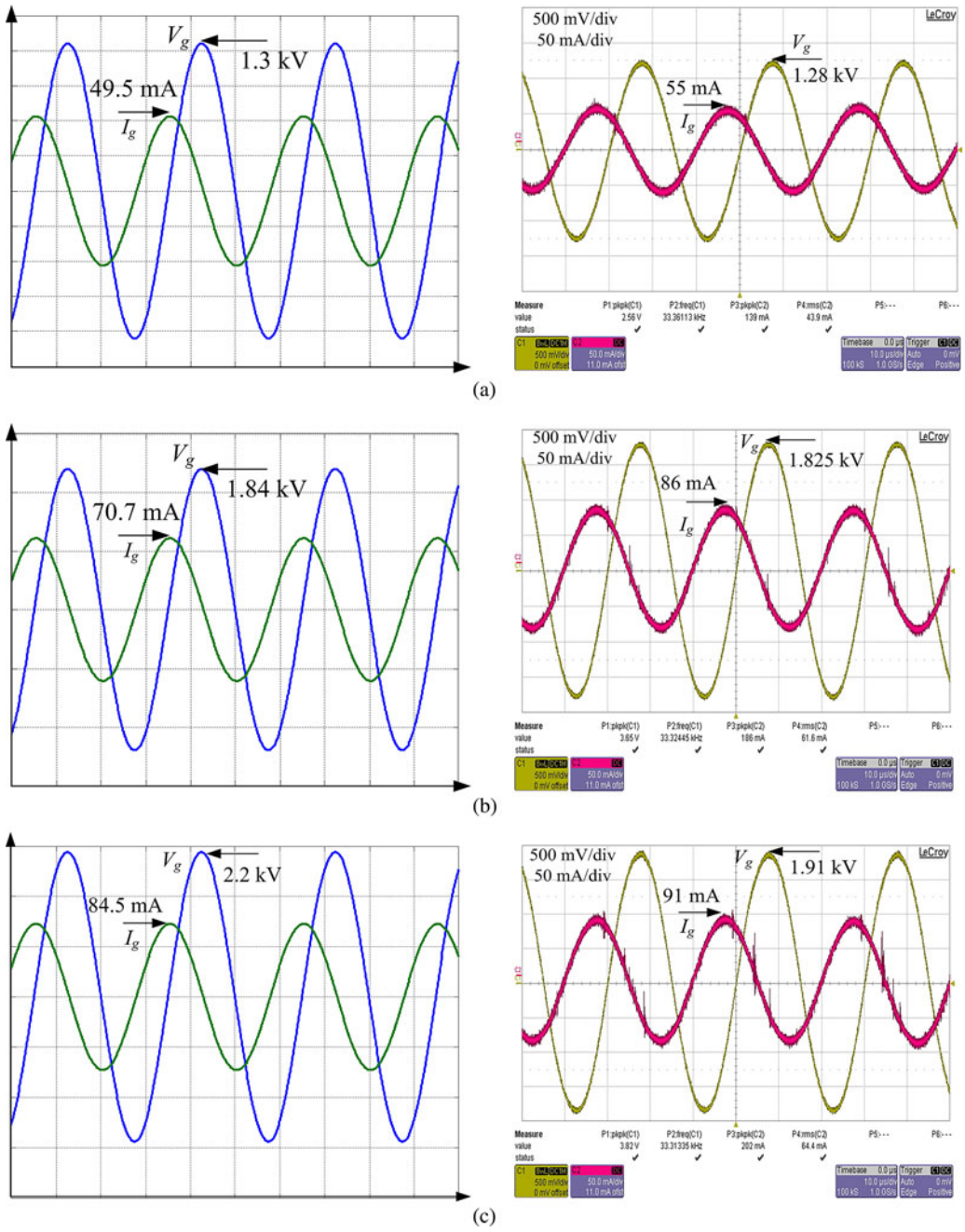

Fig. 14. Ozone chamber voltage and current waveforms at inverter input voltage of (a) 7 V, (b) 10 V, and (c) 12 V. Note: high-voltage probe scale 1000:1.

supply is normally in range of ten of ohms. Clearly, the loss of the latter is much lesser. That may explain why the efficiency of the transformerless power supply is better.

The information about the cost and size of transformer-based power supplies is not reported in the literature. However, a reasonable comparison can be justified on the basis of component count. Typically, a high-voltage power supply consists of a step-up transformer and (one or two) inductors. These inductors have values in millihenry, which are placed at primary or secondary of the transformer. Furthermore, the leakage inductance of the transformer causes high voltage spike to appear across the MOSFETs during commutation. Consequently, protection circuit is necessary to avoid switch damage. On the other hand, for the proposed transformerless power supply, two inductors (one in microhenry, the second in millihenry) and a capacitor (value in nanofarad) are used. There is no need for MOSFETs protection due to the absence of the voltage spike. As the component count of transformerless power supply is fewer, it can be assumed that cost and size of transformerless power supply will be less as compared to transformer-based power supplies.

On the issue of safety, it is notable that the galvanic isolation is absent in the transformerless systems. Inherently, there may exist a connection between the dc power supply (low-voltage side) and ozone chamber (high-voltage side). This is due to the

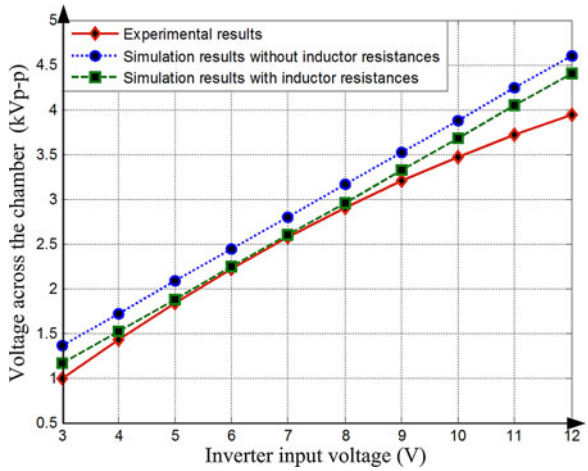

Fig. 15. Comparison of simulation and experimental results voltage across the chamber.

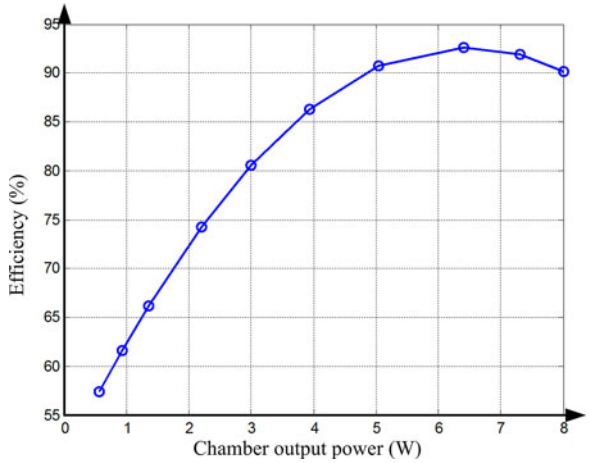

Fig. 16. Experimentally measured efficiency of power supply versus chamber output power.

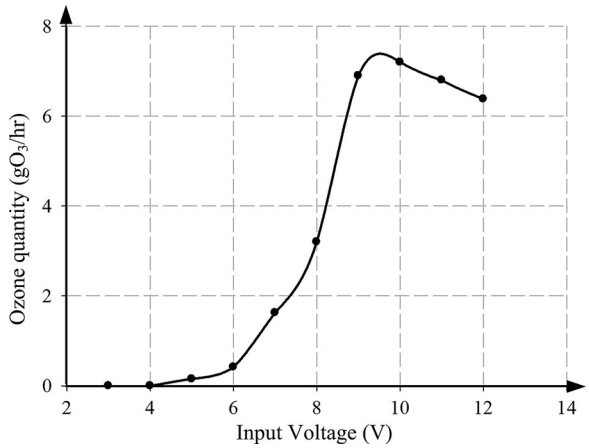

Fig. 17. Ozone quantity versus the inverter input voltage.

presence of stray capacitance between the dc power supplies to the ground that will cause common-mode voltage [47]. As a result, common-mode leakage current flows through the parasitic capacitor. To go around this problem, it is suggested that a ground fault detector may be incorporated in the circuit to fulfill the safety requirement. A ground fault detector is a reliable device that disconnects the inverter upon the detection of an isolation fault in the installation [48]. In any case, the casing for the ozone chamber is made by Acrylic Perspex sheet (with thickness of 2 mm), which has a breakdown voltage of over 10-kV rms. That should provide the sufficient insulation required for this application.

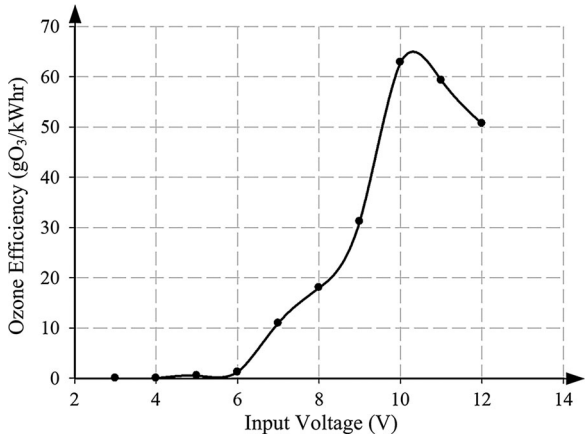

Fig. 18. Efficiency versus input voltage of inverter.

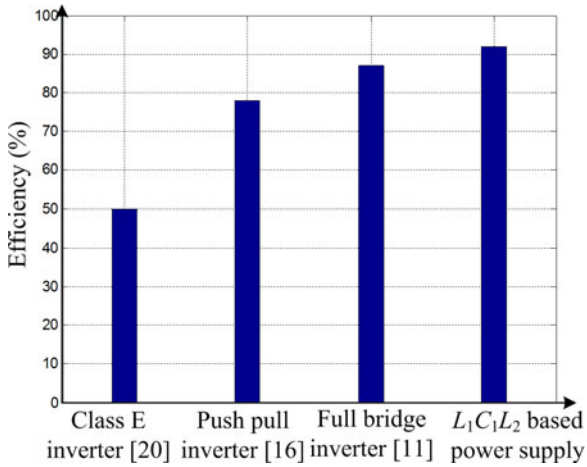

Fig. 19. Efficiency comparisons of $L_1C_1L_2$ and the transformer-based power supplies. The $L_1C_1L_2$ is tarnsformerless, while others are with transformer.

VII. Conclusion

In this paper, a $L_1C_1L_2$ resonant circuit-based power supply used in ozone generation has been investigated. Without the use of the transformer, the proposed power supply offering high voltage is capable for ozone generation. The constant phase difference between voltage and current waveforms of chamber over specific frequency range makes the open-loop operation possible. The advantage of this power supply is the reduced cost and high efficiency. Moreover, the proposed $L_1C_1L_2$ resonant circuit allows the design of high-frequency power supply to increase the power supplied to the electrode surface, which increases the ozone production. The simulation and experimental results are in good agreement and show the correctness of the design method and parameters of the proposed model.

REFERENCES

[1] X. Lei, Z. Rui, L. Peng, D. Li-Li, and Z. Ru-Juan, "Sterilization of E. coli bacterium with an atmospheric pressure surface barrier discharge," *Chin. Phys*., vol. 13, no. 1, pp. 913–917, Jun. 2004.

[2] M. V. Selma, A. Allende, F. Lopez-Galvez, M. A. Conesa, and M. I. G. Gil, "Disinfection potential of ozone, ultraviolet-C and their combination in wash water for the fresh-cut vegetable industry," *Food Microbiol*., vol. 25, no. 6, pp. 809–814, Sep. 2008.

[3] W. J. Kowalski, W. P. Bahnfleth, B. A. Striebig, and T. S. Whittam, "Demonstration of a hermetic airborne ozone disinfection system: studies on E. coli," *AIHA J. Taylor Francis*, vol. 64, no. 2, pp. 222–227, Mar. 2003.

[4] U. Kogelschatz, "Dielectric-barrier discharges: Their history, discharge physics, and industrial applications," *Plasma Chem. Plasma Process*., vol. 23, no. 1, pp. 1–46, Mar. 2003.

[5] J. L. Smilanick, "Use of ozone in storage and packing facilities," in *Proc. Washington Tree Fruit Postharvest Conf*., Wenatchee, WA, 2003, pp. 1–10.

[6] Z. Buntat, I. R. Smith, and N. A. M. Razali, "Ozone generation using atmospheric pressure glow discharge in air," *J. Phys. D: Appl. Phys*., vol. 42, no. 23, pp. 3722–3727, Dec. 2009.

[7] A. Garamoon, F. Elakshar, A. Nossair, and E. Kotp, "Experimental study of ozone synthesis," *Plasma Sources Sci. Technol*., vol. 11, no. 3, pp. 254–259, May 2002.

[8] M. A. Dimitriou, *Design Guidance Manual for Ozone Systems*. Norwalk, CT: Pan American Committee of the International Ozone Association, 1990.

[9] J. M. Alonso, J. Garcia, A. J. Calleja, J. Ribas, and J. Cardesin, "Analysis, design, and experimentation of a high-voltage power supply for ozone generation based on current-fed parallel-resonant push-pull inverter," *IEEE Trans. Ind. Appl*., vol. 41, no. 5, pp. 1364–1372, Sep. 2005.

[10] P. Hothongkham and V. Kinnares, "Measurement of an ozone generator using a phase-shifted PWM full bridge inverter," in *Proc. Int. Power Electron. Conf*., 2010, pp. 1552–1559.

[11] V. Kinnares and P. Hothongkham, "Circuit analysis and modeling of a phase-shifted pulsewidth modulation full-bridge-inverter-fed ozone generator with constant applied electrode voltage," *IEEE Trans. Power Electron*., vol. 25, no. 7, pp. 1739–1752, Jul. 2010.

[12] M. Nisoa, D. Srinoum, and P. Kerdthongmee, "Development of high voltage high frequency resonant inverter power supply for atmospheric surface glow barrier discharges," *Solid State Phenom*., vol. 107, pp. 81–86, Oct. 2005.

[13] W. Shengpei, M. Ishibashi, F. Yuelu, M. Nakaoka, and Y. Konishi, "Series-compensated inductor type resonant inverter using pulse density modulation scheme for efficient ozonizer," in *Proc Int. Conf. Power Electron. Drive Syst*., 1997, vol. 1, pp. 19–23.

[14] O. Koudriavtsev, S. Wang, Y. Konishi, and M. Nakaoka, "A novel pulse-density-modulated high-frequency inverter for silent-discharge-type ozonizer," *IEEE Trans. Ind. Appl*., vol. 38, no. 2, pp. 369–378, Mar. 2002.

[15] S. Wang, Y. Konis, M. Ishitobi, S. Shirakawa, and M. Nakaoka, "Current-source type parallel inductor-compensated load resonant inverter with PDM control scheme for efficient ozonizer," in *Proc. IEEE Int. Power Electron. Congr*., Oct. 1998, pp. 103–110.

[16] J. M. Alonso, J. Cardesin, J. A. Martin-Ramos, J. Garcia, and M. Rico-Secades, "Using current-fed parallel-resonant inverters for electro discharge applications: A case of study," in *Proc. IEEE Int. Appl. Power Electron. Conf. Expo*., 2004, pp. 109–115.

[17] J. M. Alonso, J. Garcia, A. J. Calleja, J. Ribas, and J. Cardesin, "Analysis, design and experimentation of a high voltage power supply for ozone generation based on the current-fed parallel-resonant push-pull inverter," in *Proc. IEEE Ind. Appl. Conf*., Oct. 2004, pp. 2687–2693.

[18] J. M. Alonso, C. Ordiz, D. Gacio, J. Ribas, and A. J. Calleja, "Closed-loop regulated power supply for ozone generation based on buck converter and current-fed push-pull resonant inverter," in *Proc. 13th Eur. Conf. Power Electron. Appl*., 2009, pp. 1–10.

[19] C. Ordiz, J. M. Alonso, M. A. D. Costa, J. Ribas, and A. J. Calleja, "Development of a high-voltage closed-loop power supply for ozone generation," in *Proc. IEEE Appl. Power Electron. Conf. Expo*., Feb. 2008, pp. 1861–1867.

[20] J. M. Alonso, J. Cardesin, E. L. Corominas, M. Rico-Secades, and J. Garcia, "Low-power high-voltage high-frequency power supply for ozone generation," *IEEE Trans. Ind. Appl*., vol. 40, no. 2, pp. 414–421, Mar. 2004.

[21] M. Facta, Z. bin Salam, and Z. Bin Buntat, "The development of ozone generation with low power consumption," in *Proc. Innovative Technol. Intell. Syst. Ind. Appl*., 2009, pp. 440–445.

[22] M. Ponce-Silva, J. Aguilar-Ramirez, E. Beutelspacher, J. Calderon, and C. Cortes, "Single-switch power supply based on the class E shunt amplifier for ozone generators," in *Proc. Power Electron. Spec. Conf*., 2007, pp. 1380–1385.

[23] J. M. Alonso, C. Ordiz, M. A. Dalla Costa, J. Ribas, and J. Cardesin, "High voltage power supply for ozone generation based on piezoelectric transformer," in *Proc. IEEE Int. Ind. Appl. Conf*., Sep. 2007, vol. 45, pp. 1901–1908.

[24] J. M. Alonso, C. Ordiz, M. A. D. Costa, J. Ribas, and J. Cardesín, "High-voltage power supply for ozone generation based on piezoelectric transformer," *IEEE Trans. Ind. Appl*., vol. 45, no. 4, pp. 1513–1523, Jul. 2009.

[25] T. Shao, K. Long, C. Zhang, J. Wang, D. Zhang, P. Yan, and S. Zhang, "Electrical characterization of dielectric barrier discharge driven by repetitive nanosecond pulses in atmospheric air," *J. Electrostat*., vol. 67, no. 23, pp. 215–221, May 2009.

[26] T. Shao, D. Zhang, Y. Yu, C. Zhang, J. Wang, P. Yan, and Y. Zhou, "A compact repetitive unipolar nanosecond-pulse generator for dielectric barrier discharge application," *IEEE Trans. Plasma Sci*., vol. 38, no. 7, pp. 1651–1655, Jul. 2010.

[27] U. Kogelschatz, "Filamentary, patterned, and diffuse barrier discharge," *IEEE Trans. Plasma Sci*., vol. 30, no. 4, pp. 1400–1408, Aug. 2002.

[28] M. Facta, Z. Salam, Z. Buntat, and A. Yuniarto, "Silent discharge ozonizer for colour removal of treated palm oil mill effluent using a simple high frequency resonant power converter," in *Proc. IEEE Int. Power Energy*, Nov./Dec. 2010, pp. 39–44.

[29] F. Mochammad, Z. Salam, A. Jusoh, and Z. Buntat, "Improvement in ozone generation with low voltage high frequency power converters," in *Proc. IEEE Int. Conf. Power Energy*, Dec. 2008, pp. 1446–1450.

[30] M. Teschke, D. Korzec, E. G. Finantu-Dinu, J. Engemann, and R. Kennel, "Resonant, high voltage, high power supply for atmospheric pressure plasma sources," in *Proc. IEEE Int. Power Electron. Spec. Conf*., Jun. 2004, pp. 835–839.

[31] M. Amjad, Z. Salam, M. Facta, and K. Ishaque, "Design and development of a high-voltage transformer-less power supply for ozone generators based on a voltage-fed full bridge resonant inverter," *J. Power Electron*., vol. 12, no. 3, pp. 387–398, May 2012.

[32] N. Burany, L. Huber, and P. Pejovic, "Corona discharge surface treater without high voltage transformer," *IEEE Trans. Power Electron*., vol. 23, no. 2, pp. 993–1002, Mar. 2008.

[33] R. M. Ness, S. G. E. Pronko, J. R. Cooper, and E. Y. Chu, "Resonance transformer power conditioners," *IEEE Trans. Electron Devices*, vol. 38, no. 4, pp. 796–802, Apr. 1991.

[34] A. Schönknecht and R. W. A. A. De Doncker, "Novel topology for parallel connection of soft-switching high-power high-frequency inverters," *IEEE Trans. Ind. Appl*., vol. 39, no. 2, pp. 550–555, Mar./Apr. 2003.

[35] C.-S. Wang, G. A. Covic, and O. H. Stielau, "Investigating an LCL load resonant inverter for inductive power transfer applications," *IEEE Trans. Power Electron*., vol. 19, no. 4, pp. 995–1002, Jul. 2004.

[36] S. Dieckerhoff, M. J. Ryan, and R. W. De Doncker, "Design of an IGBT-based LCL-resonant inverter for high-frequency induction heating," in *Proc. IEEE Int. Ind. Appl. Conf*., 1999, pp. 2039–2245.

[37] H. P. Pham, H. Fujita, K. Ozaki, and N. Uchida, "Phase angle control of high-frequency resonant currents in a multiple inverter system for zone-control induction heating," *IEEE Trans. Power Electron*., vol. 26, no. 11, pp. 3357–3366, Nov. 2011.

[38] M. L. G. Kissin, C.-Y. Huang, G. A. Covic, and J. T. Boys, "Detection of the tuned point of a fixed-frequency LCL resonant power supply," *IEEE Trans. Power Electron*., vol. 24, no. 4, pp. 1140–1143, Apr. 2009.

[39] H. Yoo, E. Shim, J. Kang, G. Choi, C. Lee, and B. Bang, "100 kHz IGBT inverter use of LCL topology for high power induction heating," in *Proc. IEEE Int. Power Electron*., May/Jun. 2011, pp. 1572–1575.

[40] M. Amjad, Z. Salam, M. Facta, and K. Ishaque, "A simple and effective method to estimate the model parameters of dielectric barrier discharge ozone chamber," *IEEE Trans. Instrum. Meas*., vol. 61, no. 6, pp. 1676–1683, Jun. 2012.

[41] J. M. Alonso, M. Valdés, A. J. Calleja, J. Ribas, and J. Losada, "High frequency testing and modeling of silent discharge ozone generators," *Ozone: Sci. Eng.: J. Int. Ozone Assoc*., vol. 25, no. 5, pp. 363–376, 2003.

[42] M. Ponce, J. Aguilar, J. Fernandez, E. Beutelspacher, J. M. Calderon, and C. Cortes, "Linear and non linear models for ozone generators," in *Proc. IEEE Int. Power Electron. Congr*., Oct. 2004, pp. 251–256.

[43] H. Sekiya, N. Sagawa, and M. K. Kazimierczuk, "Analysis of class DE amplifier with nonlinear shunt capacitances at any grading coefficient for high Q and 25% duty ratio," *IEEE Trans. Power Electron*., vol. 25, no. 4, pp. 924–932, Apr. 2010.

[44] I. D. Chalmers, L. Zanella, and S. J. MacGregor, "Ozone synthesis in oxygen in a dielectric barrier free configuration," in *Proc. IEEE Int. Pulsed Power Conf.*, Jul. 1995, pp. 1249–1254.
[45] J. M. Alonso, A. J. Calleja, J. Ribas, M. Rico-Secades, E. Corominas, J. Cardesin, and J. Garcia, "Low-power high-voltage universal-input inverter for ozone generation," in *Proc. IEEE Int. Power Electron. Congr.*, Oct. 2002, pp. 153–159.
[46] S. Potivejkul, V. Kinnares, and P. Rattanavichien, "Design of ozone generator using solar energy," in *Proc. IEEE Asia-Pacific Conf. Circuits Syst.*, Nov. 1998, pp. 217–220.
[47] B. Yang, L. Wuhua, G. Yunjie, C. Wenfeng, and H. Xiangning, "Improved transformerless inverter with common-mode leakage current elimination for a photovoltaic grid-connected power systems," *IEEE Trans. Power Electron.*, vol. 27, no. 2, pp. 752–762, Feb. 2012.
[48] R. Gonzalez, E. Gubia, J. Lopez, and L. Marroyo, "Transformerless single-phase multilevel-based photovoltaic inverter," *IEEE Trans. Ind. Electron.*, vol. 55, no. 7, pp. 2694–2702, Jul. 2008.

Muhammad Amjad received the B.Sc. and M.Sc. degrees in electrical engineering from the University of Engineering and Technology, Lahore, Pakistan, in 1998 and 2006, respectively. He is currently working toward the Ph.D. degree in electrical engineering at Universiti Teknologi Malaysia, Johor Bahru, Malaysia.

He has also been an Assistant Professor in the University College of Engineering and Technology, The Islamia University of Bahawalpur, Bahawalpur, Pakistan, for 11 years. His research interests include modeling of dielectric barrier discharge (DBD) chamber and power electronic converter for DBD applications.

Zainal Salam received the B.Sc. degree from the University of California, Oakland, CA, in 1985, the M.E.E. degree from Universiti Teknologi Malaysia (UTM), Johor Bahru, Malaysia, and the Ph.D. degree from the University of Birmingham, Birmingham, U.K., in 1985, 1989, and 1997, respectively.

He has been a lecturer at UTM for 25 years where he is currently a Professor in power electronics in the Faculty of Electrical Engineering. He has been involved in several research and consulting works on battery-powered converters, solar energy, and machine control. He is also the Director of the Inverter Quality Control Center, UTM, which is responsible to test photovoltaic inverters that are to be connected to the local utility grid. His research interests include all areas of instrumentation and control in renewable energy.

Mochammad Facta received the B.S. degree in electrical engineering from Universitas Hasanuddin, Makassar, Indonesia, and the M.Eng. degree from Institut Teknologi Sepuluh Nopember, Surabaya, Indonesia. He is currently working toward the Ph.D. degree at Universiti Teknologi Malaysia, Johor Bahru, Malaysia.

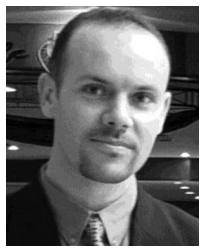

Saad Mekhilef (M'01) received the B.Eng. degree in electrical engineering from the University of Setif, Setif, Algeria, in 1995, and the M.Eng.Sc. and Ph.D. degrees from the University of Malaya, Kuala Lumpur, Malaysia, in 1998 and 2003, respectively.

He is currently an Associate Professor in the Department of Electrical Engineering, University of Malaya. He is the author or coauthor of more than 100 publications in international journals and proceedings. He is actively involved in industrial consultancy, for major corporations in the power electronics projects. His research interests include power conversion techniques, control of power converters, renewable energy, and energy efficiency.